

# Three-port measurements for determination of the effect of flow on the acoustic properties of perforates

Shail Shah<sup>1</sup>, Hans Bodén<sup>2</sup> and Susann Boij<sup>3</sup>

*Marcus Wallenberg Laboratory for Sound and Vibration Research, KTH Royal Institute of Technology, SE- 10044 Stockholm, Sweden*

Massimo D'Elia<sup>4</sup>

*Laboratoire d'Acoustique de l'Université du Mans, Le Mans, 72000, France*

A major discussion in the scientific community is the effect of the acoustic propagation direction being relative to the mean flow direction on the acoustic boundary condition posed by perforated liners. The reason being that the results from liner-impedance-education measurements show acoustic propagation upstream or downstream to the flow direction giving different resulting acoustical impedances. This paper contributes to this continuing effort to gain confidence in results obtained under different acoustical excitation and flow configurations. Instead of a traditional two-port configuration, by placing a perforate sample in a T-junction, this paper presents a three-port measurement technique. The transfer impedance of the perforate is determined under grazing as well as under normal incidence. Moreover, to study the effect of acoustic incidence relative to the flow directions, transfer impedance is also determined under the presence of grazing flow. A comparison of the measurement results with existing analytical and semi empirical models is also presented. An attempt to determine the nature of the transfer impedance under normal acoustic incidence is carried out and an analogous behavior between an empty T-junction and the perforated sample is proposed.

## I. Introduction

Perforates are used for noise control of aircraft engines as well as for other vehicles and machines. Their properties and noise reduction are known to depend on the mean flow field and other external parameters such as temperature and acoustic excitation level. Many test techniques for determining liner impedance under grazing flow conditions have therefore been developed [1-13]. There are many test rigs around the world and a number of different techniques for extracting the liner impedance from measurements have been developed. The dominating techniques, at least in terms of numbers of publications, are the so-called inverse impedance education techniques [1-10]. In order to gain confidence in the results, which may depend on both the test rig used and on the impedance education method, some comparative studies have been initiated [1, 4, 5, 8]. The in-situ impedance measurement technique [11], in which the liner is instrumented, has also been successfully applied to measure the liner impedance [12]. To study only the impedance of the perforated top sheet, methods using an impedance tube located in a side branch [14, 15] have also been used.

In this study, a three-port method similar to that proposed in Refs. [16, 17] is used to study the effect on perforate acoustic properties for different combinations of flow direction and acoustic excitation. Similar to the in-situ

---

<sup>1</sup> Ph.D. Student, Department of Engineering Mechanics; [shail@kth.se](mailto:shail@kth.se).

<sup>2</sup> Professor, Department of Engineering Mechanics, AIAA Member; [hansbod@kth.se](mailto:hansbod@kth.se).

<sup>3</sup> Associate Professor, Department of Engineering Mechanics, AIAA Member; [sboij@kth.se](mailto:sboij@kth.se).

<sup>4</sup> Ph.D. Student, Laboratoire d'Acoustique de l'Université du Mans ; [massimo\\_emiliano.delia.etu@univ-lemans.fr](mailto:massimo_emiliano.delia.etu@univ-lemans.fr)

impedance measurement technique and the side branch method, the disparities related to the Ingard-Myers boundary condition [18] are not applicable while discussing the results of the three-port method, as the boundary condition is not used for determination of the sound field in the main duct.

Acoustic properties of the sample studied here are the real part of the normalized transfer impedance, i.e., the resistance ( $\Re$ ), and the three-port scattering matrix (S-Matrix). These properties are determined with and without the presence of grazing flow. A validation of the three-port results in the absence of flow by comparing with an existing model [19] and the experimental results from impedance tube measurements [20], is presented. In the presence of grazing flow, the behavior of the calculated resistance values are compared with existing semi-empirical models [21, 22]. Moreover, similar to Ref. [17], experiments to determine the properties of an empty T-junction (test setup in the absence of a perforated sample) are also presented. This is done to determine the transfer impedance of the perforate and provide a possible explanation for the behavior of the perforate resistance in the presence of grazing flow.

## II. Experimental Technique

### A. The three-port technique

The test setup for the three-port technique can be described as an impedance tube placed in a side branch, and is inspired by studies [11, 14] which have used this type of configuration to investigate the effect of grazing flow on the impedance of perforates. The three-port measurement uses a test rig according to Figure 1, where the ducts 1, 2, and 3 intersect and form a T-junction. A perforate sample was placed covering the opening of duct 3 at the intersection of ducts 1 and 2. The end of the duct 3 was sealed to avoid leakage of grazing flow. The acoustic pressure in all three ducts was determined using the multi-microphone method [17]. Plane wave propagation over the perforated plate was assumed given that the comparison between the calculated results using the measured pressure signal and decomposed wave amplitudes at position  $P_0$ , showed good agreement. Hence, it was assumed that the total acoustic pressure at point  $P_0$  is given by  $P_0 = (P_1 + P_2)/2$ , where  $P_1$  and  $P_2$  are the total acoustic pressures at that point determined using wave decomposition in ducts 1 and 2, respectively.

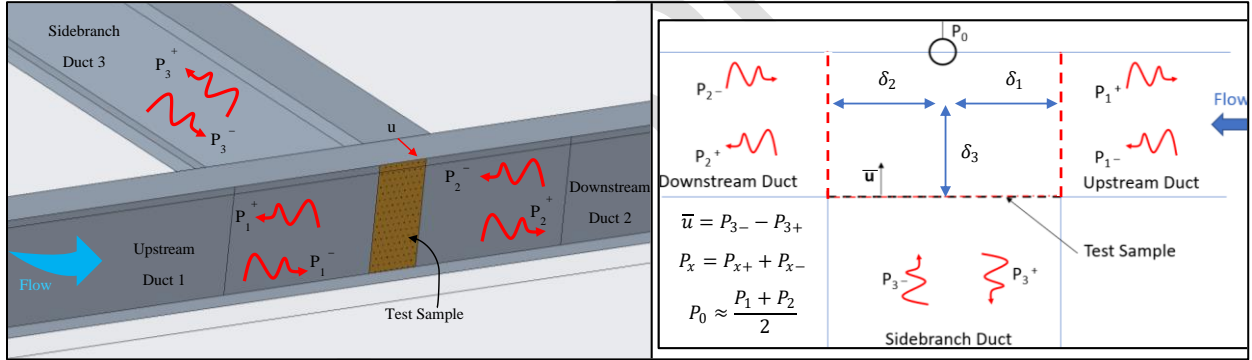


Figure 1 Schematic of the experimental setup

Using the decomposed wave pressure amplitudes, the scattering matrix (S-Matrix) of the three-port is defined as per the Eq. (1) [16]:

$$\begin{bmatrix} P_{1+} \\ P_{2+} \\ P_{3+} \end{bmatrix} = \begin{bmatrix} \rho_1 & \tau_{2 \rightarrow 1} & \tau_{3 \rightarrow 1} \\ \tau_{1 \rightarrow 2} & \rho_2 & \tau_{3 \rightarrow 2} \\ \tau_{1 \rightarrow 3} & \tau_{2 \rightarrow 3} & \rho_3 \end{bmatrix} \begin{bmatrix} P_{1-} \\ P_{2-} \\ P_{3-} \end{bmatrix}, \text{ or } \mathbf{P}^+ = \mathbf{S}\mathbf{P}^-, \quad (1)$$

where  $P_{x\pm}$  describes the decomposed wave pressure amplitudes in duct  $x$ . The direction '+' is taken outwards, and '-' is taken inwards as shown in Figure 1.  $\rho$  and  $\tau$  stand for the reflection and transmission coefficients, respectively, and the subscripts represent the respective duct. To study the properties of the sample placed in the T-junction, the origin point of the acoustical three-port must be determined. In Refs. [16, 17] the origin point is defined for an empty T-junction by studying the phase angle of transmission coefficients in absence of external flow. The geometric origin of the three-port is shifted and the alteration  $\delta$ , as shown in Figure 1, is calculated using Eq. (2) [17].

$$-2(\delta_i + \delta_j) = c \text{ mean} \left( \frac{\Delta\theta(\tau_{ij}) + \Delta\theta(\tau_{ji})}{2\pi f} \right), (i \neq j), \quad (2)$$

where  $i, j$  represent the three ducts,  $\delta_{i,j}$  are the added alterations for the respective ducts and  $\Delta\theta(\tau_{ij,ji})$  is the deviation of the phase angle of the transmission coefficients from zero. In the case when the sample is placed in the T-Junction, a modification of this method is proposed in Ref. [20]. The value of  $\delta$  is then calculated by comparing the transmission coefficients of duct 3 with the results from an impedance tube. As the sample, when viewed from duct 3, is placed in the same way as it is placed in an impedance tube, the phase angle of the transmission coefficients in both cases should be equal. Thus  $\Delta\theta(\tau_{ij,ji})$  in Eq. (2) is now changed to represent the difference in the phase angle when the sample is placed in the impedance tube and when it is placed in the T-Junction. For the perforate sample used, the values of  $\delta_1$ ,  $\delta_2$ , and  $\delta_3$  were calculated to be 15.95, 14.95 and 8.35 mm, respectively.

## B. Determination of the Transfer Impedance

The normalized transfer impedance ( $\bar{Z}$ ) of the test sample was calculated to study the acoustic properties of the sample under excitation from all three ducts, respectively. The normalization was done with respect to the characteristic impedance of air.

In the case of plane wave excitation, given that the sample is acoustically compact, it can be assumed that the normalized particle velocity ( $u$ ) is equal on both the sides of the sample. The normalized transfer impedance  $\bar{Z}$  can then be determined by taking the ratio of the pressure difference across the perforate and the acoustic particle velocity  $u$  at the sample surface, as shown in Eq. (3).

$$\bar{Z} = \frac{\Delta P}{u} = \frac{P_3 - P_0}{P_{3-} - P_{3+}} = \frac{(P_{3+} + P_{3-}) - \frac{1}{2}(P_{1+} + P_{1-} + P_{2+} + P_{2-})}{P_{3-} - P_{3+}}, \quad (3)$$

where  $P_3$  is the total acoustic pressure determined at  $\delta_3$  distance from the perforate.

Acoustic reflection from the terminations creates standing wave patterns in all the ducts, leading to the creation of nodes at the T-junction at certain frequencies. The transfer impedance calculated using Eq. (3) is dependent on the pressure at point  $P_0$ , and the presence of nodes in the vicinity of  $P_0$  lead to measurement errors [23]. The S-Matrix of the three-port describes the properties of the sample properties, independent of any termination reflections. Hence Eq. (3) can be modified to calculate  $\bar{Z}$  without the influence of termination and incorporate the S-Matrix coefficients as shown in Eqs. (4) to (6).

- 1) Considering non-reflecting terminations, in case of excitation from duct 1, we can say that  $P_{3-} = P_{2-} = 0$ . Applying it to Eq. (3) and using Eq. (1), we get:

$$\begin{aligned} \bar{Z}_1 &= \frac{\frac{1}{2}(P_{1+} + P_{1-} + P_{2+}) - P_{3+}}{P_{3+}} = \left\{ \begin{array}{l} \text{replacing } P_{1+}, P_{2+}, \text{ and} \\ P_{3+} \text{ as per Eq. (1)} \end{array} \right\} \\ &= \frac{(\rho_1 P_{1-} + P_{1-} + \tau_{1 \rightarrow 2} P_{1-})}{2\tau_{1 \rightarrow 3} P_{1-}} - 1 \Rightarrow \bar{Z}_1 = \frac{(\rho_1 + \tau_{1 \rightarrow 2} + 1)}{2\tau_{1 \rightarrow 3}} - 1 \end{aligned} \quad (4)$$

- 2) Similarly, under excitation from duct 2, we can say  $P_{3-} = P_{1-} = 0$ , and transform Eq. (3) into:

$$\begin{aligned} \bar{Z}_2 &= \frac{\frac{1}{2}(P_{1+} + P_{2-} + P_{2+}) - P_{3+}}{P_{3+}} = \left\{ \begin{array}{l} \text{replacing } P_{1+}, P_{2+}, \text{ and} \\ P_{3+} \text{ as per Eq. (1)} \end{array} \right\} \\ &= \frac{(\rho_2 P_{2-} + P_{2-} + \tau_{2 \rightarrow 1} P_{2-})}{2\tau_{2 \rightarrow 3} P_{2-}} - 1 \Rightarrow \bar{Z}_2 = \frac{(\rho_2 + \tau_{2 \rightarrow 1} + 1)}{2\tau_{2 \rightarrow 3}} - 1 \end{aligned} \quad (5)$$

- 3) Lastly, for excitation from duct 3, we assume  $P_{1-} = P_{2-} = 0$ , converting Eq. (3) into:

$$\begin{aligned} \bar{Z}_3 &= \frac{(P_{3+} + P_{3-}) - \frac{1}{2}(P_{1+} + P_{2+})}{P_{3-} - P_{3+}} = \left\{ \begin{array}{l} \text{replacing } P_{1+}, P_{2+}, \text{ and} \\ P_{3+} \text{ as per Eq. (1)} \end{array} \right\} \\ &= \frac{(\rho_3 P_{3-} + P_{3-} - \frac{1}{2}(\tau_{3 \rightarrow 1} P_{3-} + \tau_{3 \rightarrow 2} P_{3-}))}{\rho_3 P_{3-} + P_{3-}} \Rightarrow \bar{Z}_3 = \frac{1 + \rho_3}{1 - \rho_3} - \frac{1}{2} \left( \frac{\tau_{3 \rightarrow 1} + \tau_{3 \rightarrow 2}}{1 - \rho_3} \right) \end{aligned} \quad (6)$$

It should be noted that under the assumption of no absorption by the sample, Eqs. (4) to (6) can be further simplified and theoretically give the same results.

The transfer impedance of the perforate can also be determined by calculating Eq. (3) with and without the perforate present in the T-Junction. Theoretically in the absence of flow, the value of  $\bar{Z}$  should be zero for an empty T-Junction. Experimentally, marginal errors in the range of  $\approx 2\%$  were observed when comparing the calculated transfer impedance by Eq. (3) and the above-mentioned method.

As discussed in Ref. [20], an analytical model proposed by Guess [19] shows good agreement with the experimentally determined resistance of the sample in absence of external flow. The proposed model follows Eq. (7).

$$\Re = \frac{\sqrt{8\nu\omega t'}}{\sigma c d C_D}, t' = t + d, \quad (7)$$

where  $\Re$  is the resistance (real part of  $\bar{Z}$ ),  $\nu$  is the kinematic viscosity,  $\omega$  the angular frequency,  $d$  is the diameter of perforation,  $\sigma$  is the porosity,  $c$  is the speed of sound,  $C_D$  is the discharge coefficient and  $t$  is the thickness of the sample. The variable  $t'$  is the corrected length proposed and taken as the sum of  $t$  and  $d$  [19].

In the presence of grazing flow, some semi-empirical models [14, 21, 24, 25] suggest a relationship between the normalized resistance, the skin friction velocity ( $u_\tau$ ), and the frequency ( $f$ ). The model proposed by Kooi and Sarin [21] was used in this study as a reference, following Eq. (8).

$$\Re = \Re_{noflow} + \left( \frac{5 - t/d}{4\sigma c} \right) (9.9u_\tau - 3.2fd), \quad (8)$$

where  $\Re_{noflow}$  is the calculated resistance in absence of external flow as per Ref. [21].

For the case of a fully developed flow boundary layer, several models are proposed where the perforate resistance is described as a function of the mean Mach number ( $M$ ) and the porosity ( $\sigma$ ) [19, 22, 26]. The model proposed by Rao and Munjal [26] was considered in this study, following Eq. (9).

$$\Re = \frac{0.53M}{\sigma}. \quad (9)$$

In Ref. [10], results obtained using a number of different impedance reduction methods and test rigs were discussed. It was demonstrated that different transfer impedance values are obtained for upstream and downstream acoustic excitation measured for different liner samples and in different test rigs. In general, the resistance under upstream excitation shows an almost frequency-independent behavior, agreeing with the model proposed in Eq. (9). In the case of downstream excitation, a clear frequency-dependent behavior can be noted, with an almost constant decrease of the resistance with frequency, as seen in Eq. (8). Overall, the data sets show a clear difference between reduced liner resistance for upstream and downstream conditions.

### C. The Flow Profile

To determine the transfer impedance under the effect of grazing flow, characteristics of the flow profile in ducts 1 and 2 were determined. Flow speeds were controlled to give bulk velocities of Mach No.  $\approx 0.05, 0.1, 0.14,$  and  $0.19$ . Measurement of the in-duct flow profile was carried out using a pitot tube of 0.5 mm inner diameter. The flow velocity profile across ducts 1 and 2 was measured to determine the profile at three different positions vis-à-vis the sample, namely 55 mm upstream, at the center, and 55 mm downstream. Deviations of  $<2\%$  were observed between the measured velocity profiles at the three different positions. This suggests that the flow profile was not significantly affected by the presence of the sample. The bulk flow velocity ( $u_{bulk}$ ) as well as the skin-friction velocity ( $u_\tau$ ) was determined using Eq. (10) [27]. Moreover, the displacement thickness ( $\delta^*$ ) and the momentum thickness ( $\theta$ ) of the profile were determined using the Eq. (11) [28].

$$u_{bulk} = \frac{1}{H} \int_0^H u(x) dx; Re_m = \frac{u_{bulk} * H}{\nu}; u_\tau = \frac{u_{bulk} \sqrt{0.0743 (Re_m)^{-0.25}}}{2}, \quad (10)$$

$$\delta^* = \int_0^H \left( 1 - \frac{u(x)}{u_{bulk}} \right) dx; \theta = \int_0^H \frac{u(x)}{u_{bulk}} \left( 1 - \frac{u(x)}{u_{bulk}} \right) dx, \quad (11)$$

where  $H$  is the duct width,  $x$  is the distance from the smooth boundary wall, and  $Re_m$  is the Reynolds number.

The test sample under consideration is a square-edged perforate with a hole diameter and plate thickness of 1.2mm. The sample is 25 mm long in the axial direction of duct 1 and 2, 120 mm wide, and has a porosity of 2.5%. The cross section of all the three ducts is also 25 mm by 120 mm. All the measurements were performed at room temperature with deviation in the speed of sound  $<0.1\%$ . The frequency range of the measurements was 300-1500 Hz. The wave numbers considered for plane wave decomposition were calculated using a model proposed by Dokumaci [29]. NI 9234 modules were used for data acquisition at a sampling frequency of 25.6 kHz. Stepped sine excitation was used as input and reference signal. The upper limit of the incident sound pressure level was set to 120 dB to have a minimal effect of non-linearities. The frequency response function (FRF) between the measured pressure signal and the reference signal was used for the entire analysis to reduce measurement errors due to external noise. Moreover, a relative calibration of the microphones was performed to remove bias errors in the data acquisition system. A signal-to-noise ratio of  $>40$  dB was maintained during measurements conducted in the presence of grazing flow.

### III. Results

#### A. Three port results for the no flow case

The magnitude of the S-Matrix coefficients are shown in Figure 2-Figure 2a. A clear symmetry in ducts 1 and 2 can be seen. Moreover, with an increase in frequency, an increase in the reflection and subsequently a decrease in the transmission from duct 3 is observed. As per Eqs. (4) to (6), this suggests an increase in resistive behavior of the sample with an increase in frequency.

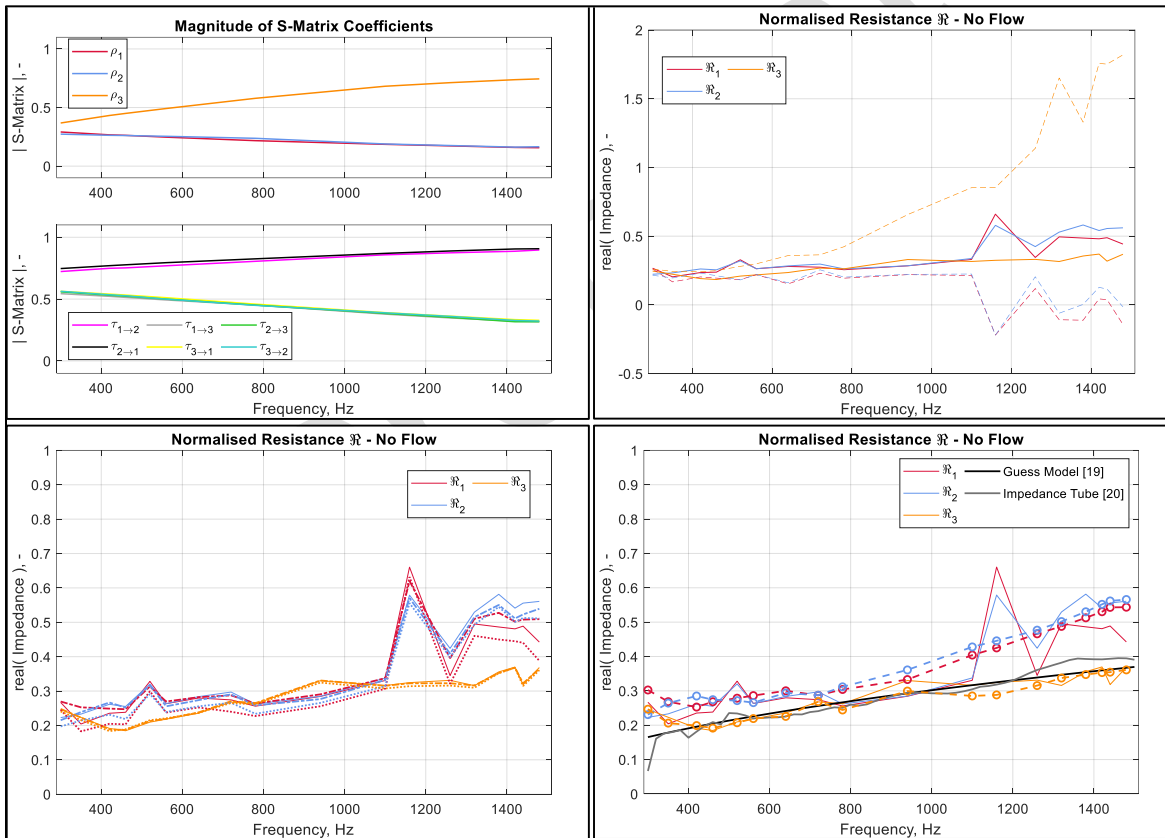


Figure 2 a) Magnitude of the reflection and transmission coefficients; b) Comparison between calculated normalized resistance, solid lines: with  $\delta_{I,III}$  from Eq. (2), dashed lines: with  $\delta_{I,III} = 0$ ; c) Comparison between normalized resistance calculated using Eq. (3), solid lines: pressure at  $P_0$  is determined using microphone signal, Dash-dot lines: pressure at  $P_0$  is determined as average of  $P_1$  and  $P_2$ , dotted lines: Difference of the calculated  $\Re$  with and without the perforate in the T-junction; d) Comparison between calculated normalized resistance and models [19, 20], solid lines: calculated using Eq. (3), circles: calculated using Eqs. (4) to (6).

Figure 2-b portrays the effect of shifting the origin of the three-port, by  $\delta_{1,2,3}$ , on the real part of the normalized transfer impedance of the perforate i.e.,  $\Re$ .  $\Re$  is determined under excitation from all three ducts to give  $\Re_1$ ,  $\Re_2$ , and  $\Re_3$ , respectively. In absence of these added alterations, calculated as per Eq. (2), a clear difference in the behavior of the resistance curves under excitation from different directions is observed. Moreover, in case of excitations from ducts 1 and 2, the resistance appears to be negative for frequencies  $>1100$  Hz, suggesting incorrect results without the addition of the calculated alterations.

As mentioned in Section II-A, to validate the accuracy of the plane wave decomposition over the perforated section a comparison of resistance is done, as shown in Figure 2 Figure 2-c. Calculation of  $\Re$  is done using Eq. (3), where in one case the value of total acoustic pressure at  $P_0$  is measured using a microphone, and in the other case it is taken as the average of the decomposed wave amplitudes in duct 1 and 2, which are evaluated at  $P_0$ . Moreover, determination of  $\Re$  is also done by taking the difference of calculated resistance with and without the perforate present in the T-junction. The resistance calculated using all the above-mentioned three methods exhibit good agreement. Given the small deviation over the frequency range, plane wave decomposition can be used for the determination of the sound field in the perforated section. The large deviations observed in the resistance curves, e.g., at  $\approx 520, 1150$  Hz can be attributed to the experimental errors caused due to standing wave patterns in the duct.

A comparison between the normalized resistance calculated using Eqs. (3) to (6) is shown in Figure 2 Figure 2-d. It should be noted that for frequencies  $>1100$  Hz, the resistance values calculated by Eq. (3) under excitation from ducts 1 and 2 are smoothed by using the S-Matrix coefficients. This is due to the removal of the effect of the termination reflections, and subsequently the measurement error due to the presence of nodes near the position  $P_0$ . A good agreement is observed between all the calculation methods, the model proposed in Eq. (7), and the resistance calculated from the impedance tube measurements [20].

## B. Flow Profile Results

Figure 3 a) Flow profile measurements using pitot tube; b) Comparison between the measured and the modelled flow velocity profiles Figure 3 displays the measured flow Mach Numbers. The displayed measurement data are the average of the values determined at three different positions with respect to the perforate. An empirical model for the measured profile is proposed in Eq. (12). (12)

$$\begin{aligned} u(x) &= 0.0145x^+ + \beta, & \text{for } 11 < x^+ < 350 \text{ in the buffer layer} \\ \frac{u(x)}{u_\tau} &= \frac{1}{0.384} \ln(x^+) + 4.27, & \text{for } 350 < x^+ < 830 \text{ in the logarithmic layer} \\ \frac{u_{max} - u(x)}{u_\tau} &= 6.3 \left( \frac{x}{H/2} \right)^2, & \text{for } 830 < x^+ \text{ in the outer zone} \end{aligned} \quad (12)$$

where  $x^+ = \frac{xu_\tau}{\nu}$  is the normalized distance from the hard wall,  $u_{max}$  is the maximum velocity (observed at the center of the cross section), and  $\beta$  is a constant determined by curve fitting of the measured data. The limits of  $x^+$  for the buffer and the logarithmic layer are defined using Ref. [30] and [31].

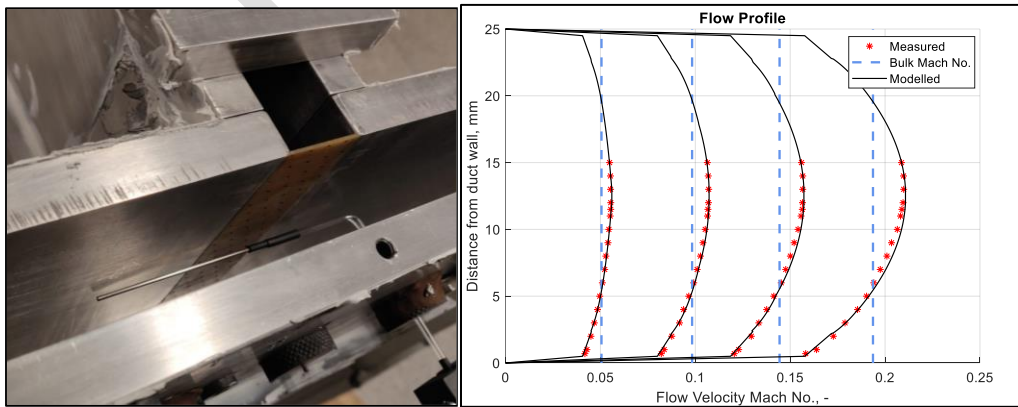


**Figure 3 a) Flow profile measurements using pitot tube; b) Comparison between the measured and the modelled flow velocity profiles**

Based on Eqs. (10) and (11), the skin friction velocity along with the different flow profile characteristics were calculated as shown in Table 1 Table 1.

Mach Number	$u_{max}$ (m/s)	$u_{bulk}$ (m/s)	$u_{\tau}$ (m/s)	$\delta^*$ (mm)	$\theta$ (mm)
0.05	19.19	17.21	0.90	9.44	2.25
0.1	36.99	33.33	1.63	6.62	3.05
0.14	54.22	48.92	2.28	3.94	2.64
0.19	72.68	65.55	2.96	1.08	0.90

**Table 1 Flow profile characteristics**

### C. Three port results under grazing flow

The magnitude of the S-Matrix coefficients and the normalized resistance calculated in the presence of grazing flow is as shown in Figure 4 Figure 4. On observing the scattering matrix coefficients, it can be clearly seen that with increasing flow velocity, the transmission from and into the duct 3 decreases and its reflection increases. This effect is due to an increase in the overall resistance of the perforate.

As displayed in Figure 4 Figure 4-b, as the flow speed increases, the resistance calculated under acoustic excitation from the grazing direction i.e.,  $\Re_{1,2}$  increase. Moreover, an increase in the flow speeds also show the resistance becoming increasingly independent of the frequency. The behavior of the curves starts following the Rao and Munjal model [26]. However, under incidence from duct 3, the resistance curve i.e.,  $\Re_3$  displays a dependence on the frequency as well as the flow speed, following the behavior seen in Ref. [21]. The reason for the discrepancy of the resistance under normal and grazing incidence with increasing flow speeds is unknown.

Moreover, on comparing with the results from impedance eduction methods [10], it is found that the distinguishing behavior of the resistance curves under upstream and downstream excitation is absent in the three-port results presented here. However, the behavior portrayed under normal incidence is similar to that of the resistance calculated using impedance eduction under downstream incidence.

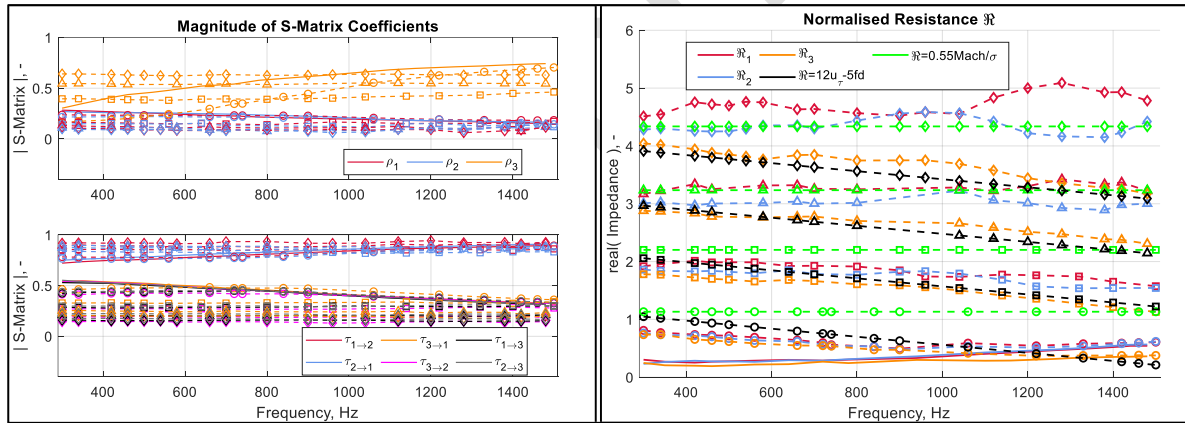


**Figure 4 a) Magnitude of S-Matrix coefficients in presence of grazing flow; b) Normalized resistance calculated in the presence of external flow compared against proposed models, solid lines: No grazing flow, circles: Mach No.  $\approx 0.05$ , squares: Mach No.  $\approx 0.1$ , triangles: Mach No.  $\approx 0.14$ , diamonds: Mach No.  $\approx 0.19$ .**

A modification to the semi-empirical model of Kooi and Sarin [21] is proposed to match the experimental results of calculated resistance. Resistance calculated as per Eq. (13) agrees well with the experimental results under normal acoustic incidence as can be seen in Figure 4 Figure 4-b. Similarly, modifying Rao and Munjal [26], Eq. (14) describes the resistance calculated under grazing incidence at higher flow speeds of Mach No.  $\approx 0.14$  and  $0.19$ ,

$$\Re = \frac{12u_{\tau} - 5fd}{\sigma c} \quad (13)$$

$$\Re = \frac{0.55Mach}{\sigma} \quad (14)$$

In order to understand the flow acoustic interaction effect on the properties of the test sample under normal incidence, the transmission coefficient and the resistance of the empty T-Junction were calculated with grazing flow and the results were compared. Scaling of the experimentally determined quantities with respect to the flow speeds was done by using Strouhal number ( $St$ ) which is calculated using Eq. (15).

$$St = fd_{eq}/U, \quad (15)$$

where  $U$  is taken as the bulk flow velocity, and  $d_{eq}$  is taken as the equivalent diameter of the rectangular pipes in case of an empty T-Junction. When the sample is placed in the T-junction,  $d_{eq}$  is taken as the diameter of the perforations. It should be noted that the diameter and the thickness of the perforated sample under consideration is equal, hence the length scaling factor is calculated using only the diameter in the analysis of the sample.

The transmission coefficients as well as the resistance of the empty T-junction calculated under normal acoustic incidence at all flow speeds is shown in Figure 5 Figure 5-a. As observed in Ref. [17], the transmission coefficients of the empty T-junction show oscillating variation with respect to the Strouhal number, indicating amplification and attenuation of the incident sound at particular Strouhal numbers. The Strouhal numbers where an amplification is displayed corresponds to intervals where the calculated resistance decreases to negative values as shown in Figure 5 Figure 5-b. Moreover, it can also be seen that the Strouhal numbers at which the resistance values equal zero are  $2^n$  multiples of a principle Strouhal number, i.e., the resistance decreases to cross zero at  $St \approx 0.44, 0.86, 1.67$ .

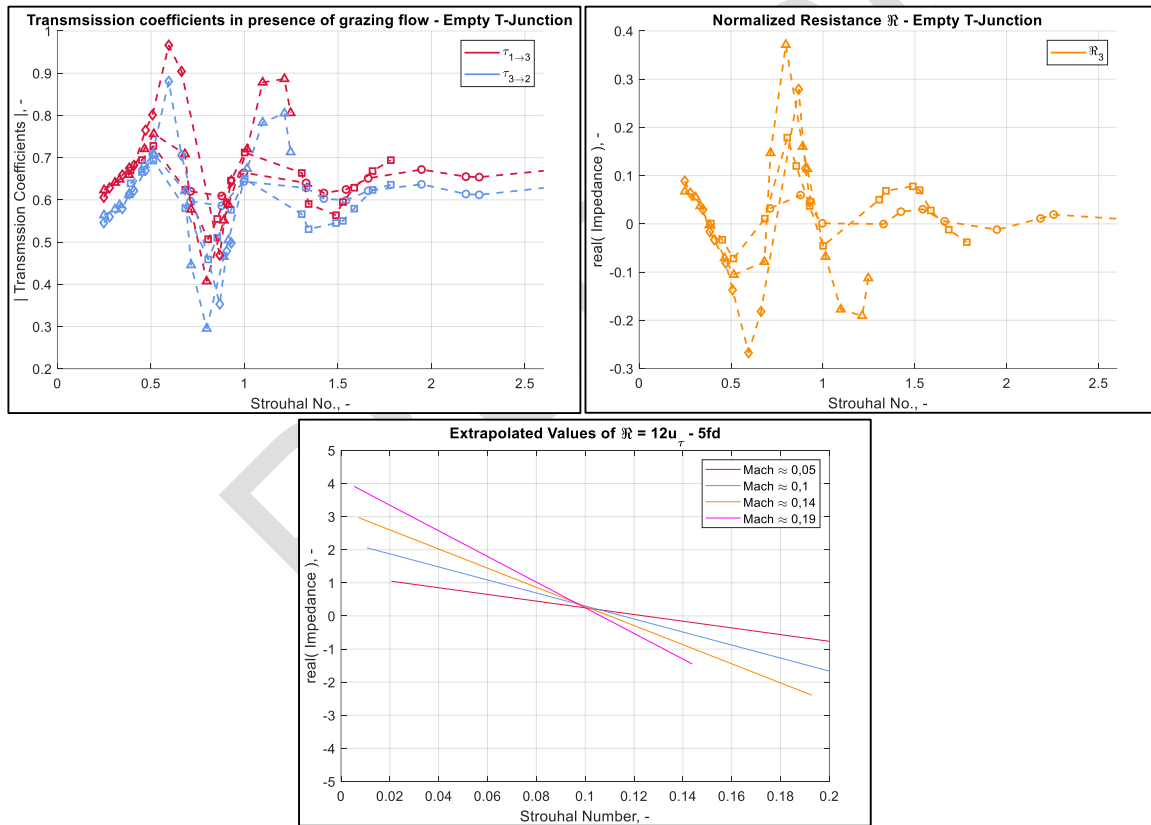


**Figure 5 a) Magnitude of the transmission coefficients of the empty T-Junction; b) Normalised resistance of the Empty T-junction calculated under normal acoustic incidence; circles: Mach No.  $\approx 0.05$ , squares: Mach No.  $\approx 0.1$ , triangles: Mach No.  $\approx 0.14$ , diamonds: Mach No.  $\approx 0.19$ ; c) Extrapolation of resistance calculated using Eq. (13) to determine the zero resistance Strouhal number.**

To compare with the perforated sample, Figure 5 Figure 5-c shows the extrapolated resistance of the perforated plate. This extrapolation is done adhering to Eq. (13), with the aim of determining the Strouhal number where the resistance of the perforated sample in presence of grazing flow becomes zero. The Strouhal Number is determined to be roughly 0.11. In case of the empty T-junction experiments, for the given frequency range all the determined

Strouhal numbers are  $> 0.25$ . On expanding the frequency range to include lower Strouhal numbers, if a fundamental is observed at  $St \approx 0.11$ , it suggests a similarity in the flow-acoustic field of an empty T-junction and a perforate under normal acoustic incidence. Moreover, in case of the perforate an approach towards an oscillating behavior, like the one observed in the empty T-junction, can also be investigated by expanding the Strouhal Number range. If observed, these similarities in the flow-acoustic field under normal acoustic incidence can be the reason for the behavior of the perforate resistance curve.

#### IV. Concluding Remarks

To study the transfer impedance of a perforated plate, an experimental three-port technique is presented in this study. Using the three-port, the acoustic properties of the perforate are studied with and without the presence of grazing flow, and under acoustic incidence from the normal and the grazing directions. To reduce the errors occurring due to termination reflections, incorporation of the scattering matrix coefficients in the calculation of the transfer impedance is displayed. In the absence of flow, agreement between the calculated resistance and an existing analytical model is found. On the addition of grazing flow, determination of the flow profile characteristics is carried out. A clear dependency of the flow velocity on the value of normalized resistance is seen and the resemblance between the behavior of the three-port results and existing semi-empirical models is shown. Modifications in the constants of the existing models are suggested to fit the experimental results. Similarities in the flow-acoustic field of an empty T-junction and a perforated section are shown. Moreover, a possible reason for the behavior of the calculated resistance curve under normal acoustic incidence is proposed. Future works include expanding the Strouhal number range to study the possibly oscillating amplification and attenuation by the perforate sample, and study the discrepancy observed in the calculated resistance under excitation from normal and grazing directions.

#### Acknowledgments



This work is part of the Marie Skłodowska-Curie Initial Training Network Pollution Know-How and Abatement (POLKA). We gratefully acknowledge the financial support from the European Commission under call H2020-MSCA-ITN-2018 (project number: 813367).

#### References

- [1] Jones, M. G., Parrott, T. L., and Watson, W. R., *Comparison of Acoustic Impedance Education Techniques for Locally-Reacting Liners*, in *9th AIAA/CEAS Aeroacoustics Conference*. 2003: Hilton Head, South Carolina. p. 1837-1847.
- [2] Watson, W. R. and Jones, M. G. , *Comparison of Convected Helmholtz and Euler Model for Impedance Education in Flow*, in *12th AIAA/CEAS Aeroacoustics Conference*. 2006: Cambridge, Massachusetts.
- [3] Jones, M.G., Watson, W.R., and Nark, D.M., *Effects of Flow Profile on Educated Acoustic Liner Impedance*, in *16th AIAA/CEAS Aeroacoustics Conference*. 2010: Stockholm, Sweden.
- [4] Jones, M.G. , Watson, W.R., Howerton, B.M. and Busse-Gerstengarbe, S., *Comparative study of Impedance Education Methods, art 2: NASA Tests and Methodology*, in *19th AIAA/CEAS Aeroacoustics Conference*. 2013.
- [5] Watson, W.R., and Jones, M. G, *A Comparative Study of Four Impedance Education Methodologies Using Several Test Liners*, in *19th AIAA/CEAS Aeroacoustics Conference*. 2013: Berlin, Germany.
- [6] Elnady, T., Bodén, H., and Elhadidi, B., *Validation of an Inverse Semi-Analytical Technique to Educate Liner Impedance*. AIAA Journal, 2009. **47**: p. 2836-2844.
- [7] Busse-Gerstengarbe, S., Richter, C., Lahiri, C., Enghardt, L., Roehle, I., Thiele, F., Ferrante, P., and Scofano, A., *Impedance Education Based on Microphone Measurements of Liners under Grazing Flow Conditions*. AIAA Journal, 2012. **50**: p. 867-879.
- [8] Zhou, L., Bodén, H., Lahiri, C., Bake, F., Enghardt, L. and Elnady, T., *Comparison of impedance education results using different methods and test rigs*, in *20th AIAA/CEAS Aeroacoustics Conference*. 2014: Atlanta, GA.
- [9] Kabral, R., Bodén, H. and Elnady, T., *Determination of Liner Impedance under High Temperature and Grazing Flow Conditions*, in *20th AIAA/CEAS Aeroacoustics Conference*. 2014: Atlanta, GA.
- [10] Bodén, H., Zhou, L., Cordioli, J., Medeiros, A. and Spillere, A., *On the effect of flow direction on impedance education results*, in *22nd AIAA Aeroacoustics Conference*. 2016.
- [11] Dean, P.D., *An In-Situ method of wall acoustic impedance measurements in flow ducts*. Journal of Sound and Vibration, 1974. **34**: p. 97-130.

- [12] Zandbergen, T., *On the Practical Use of Three-Microphone Technique for In-Situ Acoustic Impedance Measurements on Double Layer Flow Duct Liners*, in *7th AIAA Aeroacoustics Conference*. 1981.
- [13] Gaeta, R.J., Mendoza J.M. and Jones M.G., *Implementation of in-situ impedance techniques on a full scale aero-engine system*, in *13th AIAA Aeroacoustics Conference*. 2007.
- [14] Dickey, N.S., Selamet, A. and Ciray, M.S., *An experimental study of the impedance of perforated plates with grazing flow*. Journal of Acoustical Society of America, 2001. **110**: p. 2360-2370.
- [15] Feder, E. and Dean, L. W., *Analytical and Experimental Studies for Predicting Noise Attenuation in Acoustically Treated Ducts for Turbofan Engines NASA Contractor Report CR-1373* 1969.
- [16] Karlsson, M. and Åbom, M., *Aeroacoustics of T-junctions-an experimental investigation*. Journal of Sound and Vibration, 2010. **329**: p. 1793-1808.
- [17] Holmberg, A., Karlsson, M. and Åbom, M., *Aeroacoustics of rectangular T-junctions subject to combined grazing and bias flows - An experimental investigation*. Journal of Sound and Vibration, 2015. **340**: p. 152-166.
- [18] Myers, M.K., *On the Acoustic Boundary Condition in the presence of Flow*. Journal of Sound and Vibration, 1980. **71**: p. 429-434.
- [19] Guess, A.W., *Calculation of Perforated Plate Liner Parameters from Specified Acoustic Resistance and Reactance*. Journal of Sound and Vibration, 1975. **40**: p. 119-137.
- [20] Shah S., Bodén H. and Boij, S., *Experimental Study on the Acoustic Properties of Perforates under Flow using Three-Port Technique*, in *27th International Congress on Sound and Vibration*. 2021 (unpublished).
- [21] Kooi, J.W. and Sarin, S.L., *An experimental study of the acoustic impedance of Helmholtz resonator arrays under a turbulent boundary layer*, in *7th AIAA Aeroacoustics Conference*. 1981.
- [22] Rice, E.J. , *A Model for the acoustic impedance of a perforated plate liner with multiple frequency excitations* 1971.
- [23] Åbom, M. and Bodén, H. , *Error analysis of two-microphone measurements in ducts with flow*. Journal of Acoustical Society of America, 1988. **83**: p. 2429-2438.
- [24] Kirby, R. & Cummings, A., *The impedance of perforated liners subjected to grazing flow and backed by porous media*. Journal of Sound and Vibration, 1998.
- [25] Cummings, A., *The effects of Grazing Turbulent Pipe-Flow on the Impedance of an Orifice*. Acoustica, 1986. **61**: p. 233-242.
- [26] Rao, N. and Munjal, M., *Experimental evaluation of Impedance of perforates with Grazing Flow* Journal of Sound and Vibration, 1986.
- [27] Zanoun, E-S, Nagib,H. and Durst, F., *Refined cf relation for turbulent channels and consequences for high-Re experiments*. Fluid Dynamics Research, 2009. **41**.
- [28] Schlichting, H., *Boundary Layer Theory*. 1968: McGraw-Hill Inc.
- [29] Dokumaci, E., *A Note on Transmission of Sound in a Wide Pipe with Mean Flow and Viscothermal Attenuation*. Journal of Sound and Vibration, 1997. **208**: p. 653-655.
- [30] Lee, M. and Moser, R., *Direct numerical simulation of turbulent channel flow up to  $Re\tau\approx 5200$* . Journal of Fluid Mechanics, 2015. **774**: p. 395-415.
- [31] Zhou, L., *Acoustic characterization of orifices and perforated liners with flow and high-level acoustic excitation*, in *MWL Sound and Vibration*. 2015, KTH Royal Institute of Technology.